Surface & Coatings Technology 497 (2025) 131737

Contents lists available at ScienceDirect

Surface & Coatings Technology

journal homepage: www.elsevier.com/locate/surfcoat

Does the dispersion method affect the tribological properties of graphene oxide?

Chang Tu [a], Rui Yuan [a,*], Huiping Qi [a], Lei Chen [b], Xiaoyuan Qin [c], Jing Yuan [d]

[a] Salt Lake Chemical Engineering Research Complex, College of Chemical Engineering, Qinghai University, Xining 810016, China
[b] State Key Laboratory of Solid Lubrication, Lanzhou Institute of Chemical Physics, Chinese Academy of Sciences, Lanzhou, China
[c] State Key Laboratory of Plateau Ecology and Agriculture, Qinghai University, Xining 810016, China
[d] Qinghai Provincial Key Laboratory of Nanomaterials and Technology, Qinghai Minzu University, Xining, Qinghai 810007, China

ARTICLE INFO

Keywords:
Graphene oxide
Flake size
Ultrasonic frequency
Friction performance
Molecular dynamics simulation

ABSTRACT

Why do the tribological properties of graphene-based nanomaterials vary widely in different reports? Could this possible be due to different dispersion methods? To address this problem, we prepared four types of graphene oxide (GO): GO-1 (mechanical stirring, 2 h), GO-2 (ultrasonic, 10 kHz, 2 h), GO-3 (ultrasonic, 20 kHz, 2 h) and GO-4 (ultrasonic, 40 kHz, 2 h). AFM measurements revealed that the dispersion method had a significant effect on the thickness and size of the flakes, especially the size, which were 1691.7 ± 1148.6 μm2 (GO-1), 313.0 ± 144.7 μm2 (GO-2), 48.0 ± 17.5 μm2 (GO-3) and 20.7 ± 7.8 μm2 (GO-4). Combined with XPS, FTIR and Raman analysis, dispersion method has no significant effect on the chemical properties of GO, but slightly increases the content of epoxy groups on the surface of its flakes. Friction test showed that the smallest GO-4 coatings have the best wear resistance due to the formation of a larger and denser lubricant film. MD simulation results further revealed the relationship between flake size and tribological properties by investigating the changes of GO-300 (big) and GO-100 (small) during surface enrichment, load down and sliding. It was found that the better substrate coverage, homogeneous dispersion, lower frictional resistance and better defect self-repairing ability of GO-100 may be the main reasons for their good wear resistance. Thus, our study provides a theoretical basis for the selecting the dispersion method of layered materials.

1. Introduction

Friction and wear are one of the main causes of large energy losses and component failures in moving mechanical devices [1]. Graphene offers unique properties as a solid lubricant and is expected to be used as an ultra-thin coating material for surfaces, virtually inhibiting energy consumption in mechanical components [2–6]. Nowadays, many reports have demonstrated that graphene can achieve macroscale superlubricity, such as Ali Erdemir' group [7], Jianbin Luo' group [8], Quanshui Zheng's group [9], Li Ji' group [10], Junyan Zhang' group [11] and so on. Besides, the effects of external ambient humidity [12], substrate surface [13], synergetic effect [14] and various types of atmospheric environments [15] on the superlubricity of graphene were also investigated. However, the excellent lubrication properties of graphene depend on its specified 2D structure, but such specified structures synthesized by chemical vapor deposition [16] or specific mechanical and chemical exfoliation methods [17] are very complex and expensive, making them difficult to achieve in practical working conditions. In addition, due to the lack of functional groups, graphene is difficult to attach to solid substrates, leading to extreme peeling and failure during friction.

Graphene oxide (GO) is the product of graphene oxidation treatment, and the introduction of oxygen-containing functional groups can endow GO with hydrophilicity and good surface activity. The oxygen-containing groups on the flakes can enhance sliding resistance and increases the friction coefficient, but their better interfacial bonding effectively increase the friction life of the corresponding coating [18]. Sun et al. investigates the interfacial behavior of multilayer GO films by GO-to GO friction force microscopy, where the method of dispersing GO is magnetic string [19]. Ji et al. determines the effect of humidity on the frictional behavior of GO and find its friction coefficient is reversible in alternating humidities environments, and their dispersion of GO is carried out using ultrasonic (2 h) [20]. Li et al. fabricates GO/MoS_2 flakes films on stainless steel by a simple electrophoretic deposition method in

* Corresponding author.
E-mail address: yuanruiqhdx@163.com (R. Yuan).

https://doi.org/10.1016/j.surfcoat.2025.131737
Received 25 November 2024; Received in revised form 23 December 2024; Accepted 3 January 2025
Available online 5 January 2025

water, achieving a significant increase in wear resistance, using ultrasonic dispersion of the nanomaterials [14]. Previous studies have shown that GO is a promising lubricant maternal with good wear resistance. However, it is worth noting that although all the above reports investigated the tribological properties of GO, they used different GO dispersion methods, such as magnetic stirring and ultrasonic. In fact, the details of dispersion treatment are usually neglected in many articles [21–23], and in particular the ultrasonic frequency is almost rarely mentioned. So, the question arises: does the dispersion method have any effect on the structure, chemical properties and tribological performances of nanomaterial and how does it proceed?

To address the above issues, our paper prepares different frequencies of ultrasonic (10 kHz, 20 kHz and 40 kHz) and mechanical stirring to prepare GO with different dispersion methods. Experiments combined with molecular simulation methods are used to systematically investigate the effects of dispersion methods on the molecular structure, chemical properties and wear resistance of GO coatings.

2. Experimental

2.1. Materials

Graphene oxide was purchase from NanJing JI Cang Nano Technology Co.Ltd. (Nan Jing, China). Anhydrous ethanol was obtained from Maclean's Biochemical Technology Co. Ltd. (Shanghai, China). Other chemical reagents were all analytical grade and used without further purification. Monocrystalline silicon chip (20 mm × 20 mm, thickness of 650 μm) was purchased from Zhejiang Lijing Technology Co. Ltd. (Zhejiang, China).

2.2. Characterizations

The chemical states and crystallographic structures of the GO-based flakes were investigated by an X-ray photoelectron spectroscope (XPS, ESCALAB, Thermo Fisher, USA) with ionized source Laser and sizes 400 μm, X-ray diffraction (XRD, D-max2500PC Rigaku, Japan) with copper target and Raman spectroscopy (InVia Qontor, Renishaw, UK) with a laser of 532 nm, exposure time 1 s and laser power 5 %. The surface morphologies and the elemental distributions of GO and its coatings were obtained by Optical 3D surface profiler (SuperView W1 CHOTEST, China), Scanning electron microscopy (SEM, JSM-6610LV, Japan (EDS; secondary electron)) with voltage15 KV and Wd = 10 cm, transmission electron microscopy (TEM, JEM-2100F, 200 kV Japan). The thickness of the flakes was investigated by Atomic Force Microscope (AFM, Dimension ICON, Bruker, USA) with automatic mode. Thermal stability of the nanocomposites was determined by thermogravimetric analysis (TGA, STA449F3-DSC200F3, netzsch, Germany) with a nitrogen atmosphere from room temperature to 800 °C at a heating rate of 10 °C/min.

The tribological performance of the GO-based coating was analyzed by MS-T3001 tribometer (Lanzhou Huahui Instrument Technology, China). In the experiment, a stainless ball (GCr15, 6 mm diameter Ra = 20 nm 66HRC) was rotated over the coating. The loads were set to 0.1 N, 0.5 N and 1 N, radius of 5 mm and the rotation speed of 200 r/min. The friction tests of all coatings were performed in vacuum environment (Vacuum level < −0.08) at room temperature (around 25 °C, humidity 30 %). All the tests were carried out three times under the same conditions to ensure performance stability.

2.3. Preparation

2.3.1. Preparation of GO with different ultrasonic frequency

GO flakes with different sizes and exfoliation degrees were prepared by controlling the ultrasound frequency. Specifically, 0.5 g of GO was dispersed in 100 mL of ethanol, repeated four times, followed by mechanically stirred for 2 h, ultrasonicated at frequency of 10 kHz for 2 h, ultrasonicated at frequency of 20 kHz for 2 h, and ultrasonicated at frequency of 40 kHz for 2 h and labeled as GO-1, GO-2, GO-3 and GO-4.

2.3.2. Preparation of GO coating

The monocrystalline silicon wafers were ultrasonicated in acetone and ethanol for 0.5 h, dry nitrogen blow-dry, and then fixed on the surface of the steel block. The fresh GO/ethanol mixture prepared as described previously was sprayed on the silicon wafers with a spray gun (RG-3 L, ANEST IWATA Corporation, Japan) operating with the high purity nitrogen with 0.2 MPa, followed by vacuum drying at 80 °C. Thickness of the GO coatings were about 1.5 μm (Fig. S1).

2.4. Theoretical calculations

The MD model consisted of two types of GO, namely GO-100 and GO-300, representing the number of carbon atoms of GO as 100 and 300. Based on the XPS data, the ultrasonic treatment had a small effect on the degree of oxidation of GO, so the content of epoxy, hydroxyl, ketone and carboxyl groups in GO were specified to be 15 %, 6 %, 9 % and 4 % (Table S1). The mass of GO in the above two systems were controlled to be essentially the same, and number of GO flakes added in GO-100 and GO-3 were 6 and 18, respectively. To study the friction process, the Fe (100) metal surface was selected as the upper and lower sliding interfaces [24,25]. Among them, the GO-based systems were bult as a middle layer and the Fe layers both above and below were fabricated. The detail molecular structure was depicted in Fig.S2.

The geometric optimization of the computational model and subsequent kinetic calculations were performed using the COMPASS (Condensed-phase Optimized Molecular Potentials for Atomistic Simulation Studies) force field [26]. The simulation temperature was implemented by Nóse-Hoover thermostat (excluding the direction of sliding from the temperature calculation) with a Q ratio of 0.01 [27,28]. The Atom based method and Ewald method were used to calculate the van der Waals and the long-range electrostatics of simulation [29]. All initial structures were first geometrically optimized using the Smart algorithm, followed by the NVT dynamic is performed in 1 ns (time step 0.25 fs) and 4 ns (time step 0.5 fs), an addition NPT dynamic was run for 1 ns at a corresponding pressure of 0.2 GPa [30,31]. The above systems were then subjected to a NVT simulation for 1 ns, followed by confined shear with velocity of 0.04 Å/ps (1 ns, 0.2 fs).

3. Results and discussion

3.1. GO-based flakes analysis

Fig. 1 shows the SEM and TEM morphology of GO-1, GO-2, GO-3 and GO-4. The un-sonicated GO-1 are thicker and larger, and their SAED patterns show a typical ring (multilayer structure) with a layer spacing of about 0.66 Å [32]. After ultrasonic treatment, the GO-2, GO-3 and GO-4 are significantly thinned and possessed clear diffraction spots, and the layer spacing are slightly increased to around 0.72 Å, indicating that the introduction of ultrasound facilitates the formation of a looser structure [33,34]. In addition, the exfoliation degree of the flake gradually increases with increasing ultrasonic frequency, especially for GO-4, whose SAED patterns appeared as a distinctive hexagonal spot, suggesting the possible formation of a monolayer. It is worth noting that the diameter of the GO flakes also decreases from GO-1(64 μm) to GO-4 (9.5 μm).

The effects of different ultrasound frequencies on the exfoliation degrees and sizes are investigated using AFM [35,36]. As shown in Fig. 2a-c, the GO-1 are very large and there is obvious stacking between the flakes. After a smaller frequency of ultrasound, the exfoliation of GO increases significantly and the layers are thin and large (GO-2). Continuing to increase the ultrasound frequency, the exfoliation degree of the flakes does not change significantly, but their size decrease rapidly (GO-3 and GO-4). Further statistics on the thickness and size of each sheet (approximately 100) are shown in Figs. 2e and S3–6. It is not

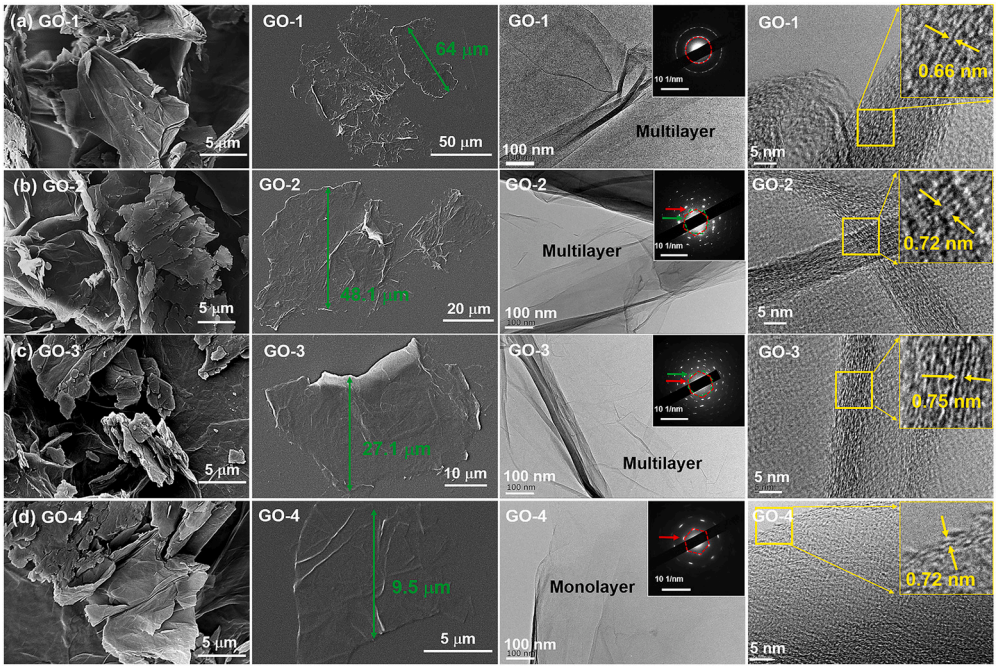

Fig. 1. Micromorphology of GO-1 (a), GO-2 (b), GO-3 (c) and GO-4 (d). SEM images; TEM images and the corresponding SAED.

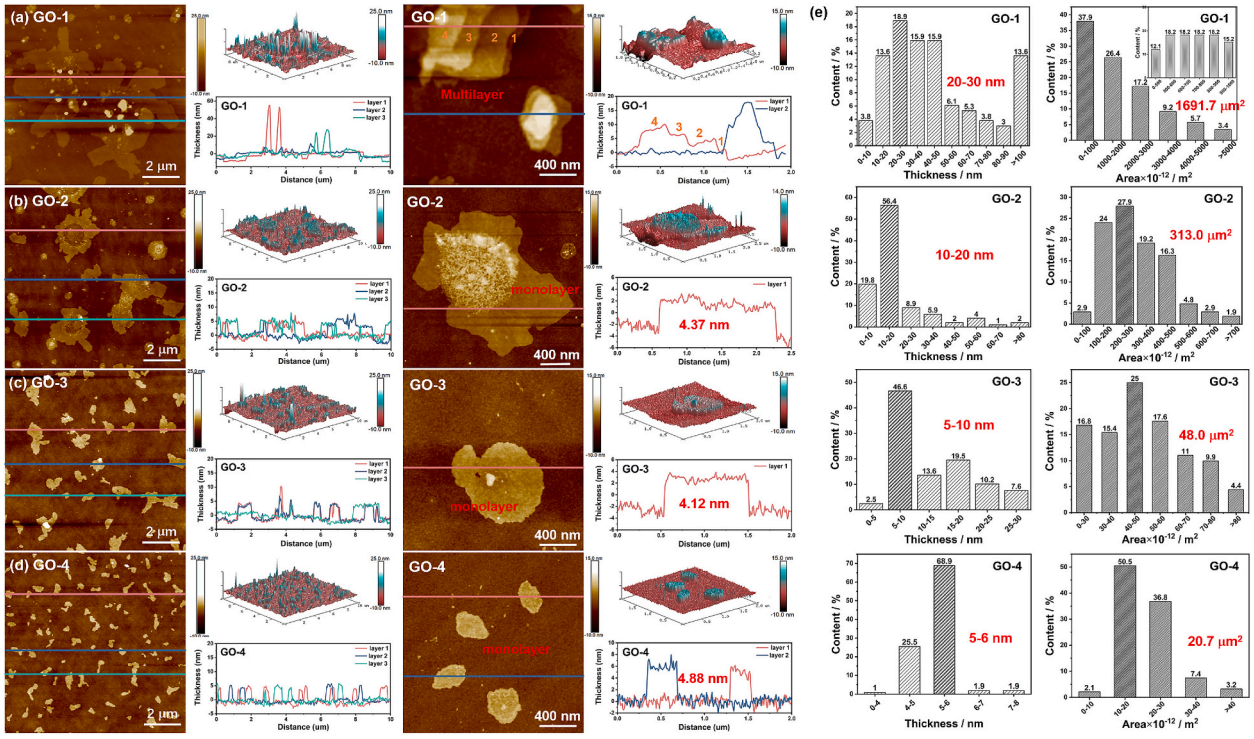

Fig. 2. (a-d) AFM images and corresponding height profiles of GO-1, GO-2, GO-3 and GO-4. (e) Thickness and area distribution of GO-1, GO-2, GO-3 and GO-4.

different to find that from GO-1 to GO-4, the exfoliation degree of the flakes gradually increases, while the size of the flake decreases dramatically. In terms of thickness, GO-1 has the most dispersed thickness distribution, with the highest percentage of 4–6 layers at 18.9 %, but there are still 13.6 % of flakes with more than 25 layers, which indicates that GO without ultrasonically dispersed is very heterogeneous. After dispersion in ultrasound at 10 kHz for 2 h, the thickness of flakes decreases significantly and become more regular, with 56.4 % stacked in 2–3 layers. While GO-3 and GO-4 are basically monolayer structures, indicating that 20 kHz ultrasonic is sufficient to achieve better dispersion and exfoliation of flakes. Surprisingly, the effect of ultrasound on the size of flake is tremendous. From GO-1 to GO-4, the areas of the flakes are 1691.7 ± 1148.6 μm^2, 313.0 ± 144.7 μm^2, 48.0 ± 17.5 μm^2 and 20.7 ± 7.8 μm^2 (Fig.S7). Thus, prolonged and high-frequency sonication does produce flakes of smaller size and uniform distribution.

The structural and chemical properties of GO-1, GO-2, GO-3 and GO-4 are further investigated and shown in Fig. 3. XPS analysis shows that the atomic content ratio of C to O on the surface of GO decreases with the

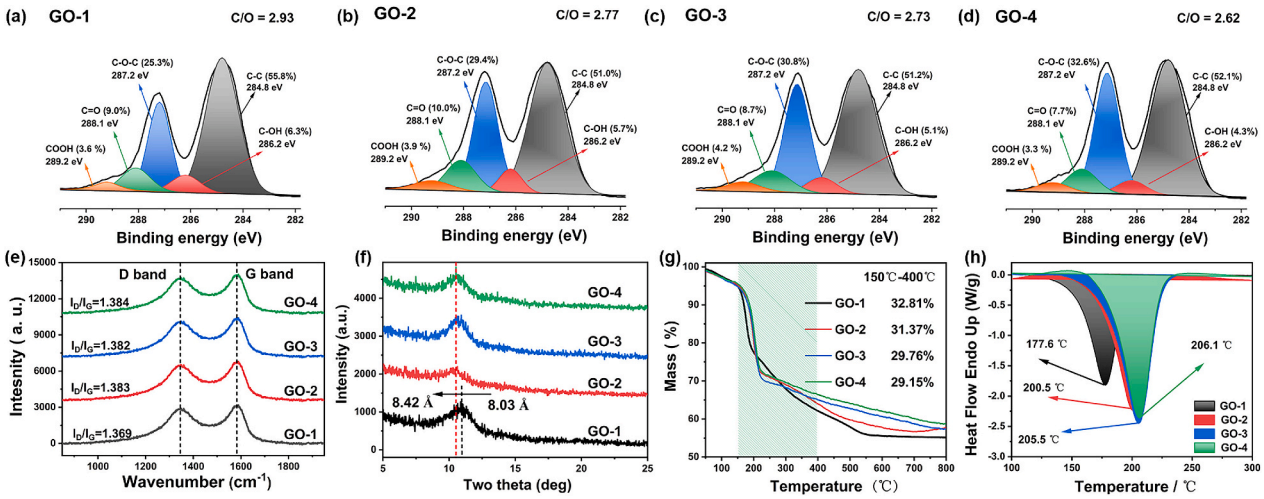

Fig. 3. Characterization of the GO-1, GO-2, GO-3 and GO-4. (a-d) XPS C 1 s; (e) Raman; (h) XRD; (g-h) TG and DSC.

increase of the sonication frequency from 2.93 (GO-1) to 2.62 (GO-4) (Fig.S8), which indicates that sonication treatment increases the content of oxygen-containing functional groups on the GO sheets. Statistically, the epoxy groups on the surface of flakes increase the most, from 25.5 % to 32.6 % [37]. The Raman spectra of GO show two strong bands: the G band at 1583 cm^{-1} is due to first order scattering of the E2g mode (sp^2 hybridization), and the D band at 1340 cm^{-1} is attributed to the presence of defects (sp^3 defect or disorder) in the GO [38,39]. It is found that the variation of $I_{(D)}/I_{(G)}$ was related to the oxidation level, the higher oxidation degree result in an increase in the $I_{(D)}/I_{(G)}$ ratio. As shown in Fig. 3e, it increases from 1.369 to 1.384, further confirming that strong sonication increases the oxidation of GO. In addition, the structures of flakes are investigated using X-ray diffraction (XRD) analyses (Fig. 3f). In agreement with previous TEM results, the interlayer spacing of GO increases significantly after sonication, from 8.03 Å (GO-1) to 8.42 Å (GO-4) [40–42]. This increase in interlayer spacing facilitates easier desorption of interlayer water from GO flakes during drying, thereby improving thermal stability. As shown in Fig. 3g-h, the thermal decomposition temperature of GO-1, GO-2, GO-3 and GO-4 are 177.6 °C, 200.5 °C, 205.5 °C and 206.1 °C. However, the effect of ultrasonic dispersion on the structural and chemical properties of GO is not very significant and only slightly increases the content of epoxy groups on the surface of its flakes.

Based on above studies, the effects of dispersion methods on the GO

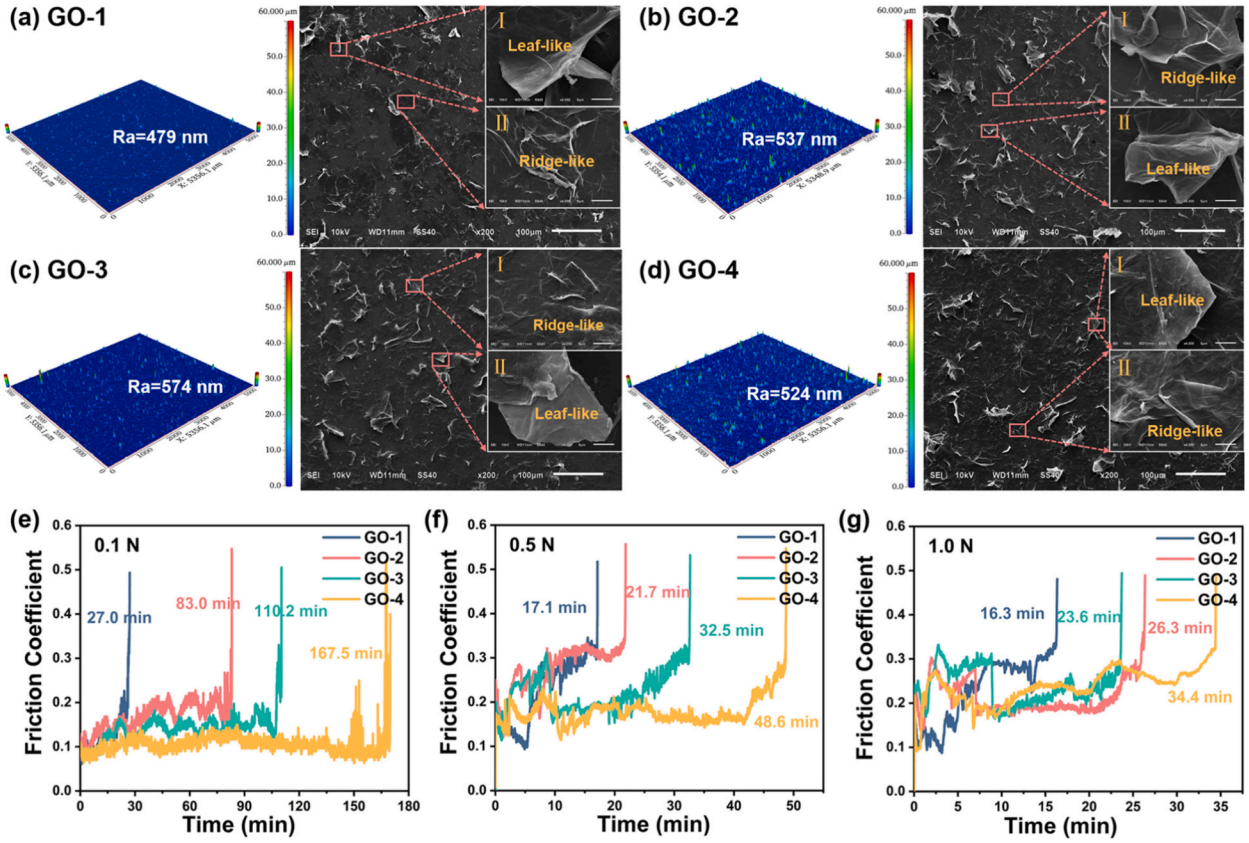

Fig. 4. 3D topographies and SEM images of GO-1, GO-2, GO-3 and GO-4 (a-d). friction curve of GO coating under 0.1 N, 0.5 N and 1.0 N (e-f).

are mainly focused on the following aspects: (1) Compared with mechanical stirring, ultrasonic dispersion can improve the degree of exfoliation of the flakes, in which 20 kHz ultrasound can lead to a better degree of exfoliation of GO. (2) high-frequency ultrasound enables the GO to form smaller sizes; (3) Ultrasound increases the content of epoxy groups on the GO. Among them, the choice of dispersion method has the greatest influence on the size of flakes.

3.2. Tribological properties of GO-based coatings

Fig. 4a-d show the surface morphology of GO-1, GO-2, GO-3 and GO-4. It is found that the surfaces of these types of coatings are relatively flat, with the surface roughness of 479 nm, 537 nm, 573 nm and 524 nm [43,44]. However, the surface of the GO-1 (without ultrasonic) is the flattest in comparison. The SEM studies reveal that the surface of the coating contains more small burrs, and the ultrasonically treated coatings have more burrs on the surface. These burrs can be differentiated into two types, bulging (ridge-like) and partial peeling (leaf-like). Consequently, larger and thicker flakes may tend to be enriched on the metal surface in a regular manner.

The coefficient of friction (COF) of the GO-1, GO-2, GO-3 and GO-4 coatings at 0.1 N, 0.5 N and 1.0 N are shown in Fig. 4 (e-g). It is not difficult to find a large gap between the tribological properties of these coatings. From 0.1 N to 1.0 N, the GO-4 coating has the longest friction life, while GO-1 has the shortest friction life, which is 167.5 min (GO-4), 110.2 min (GO-3), 83 min (GO-2) and 27 min (GO-1) at 0.1 N, 48.6 min (GO-4), 32.5 min (GO-3), 21.7 min (GO-2) and 17.1 min (GO-1) at 0.5 N, 34.4 min (GO-4), 26.3 min (GO-3), 23.6 min (GO-2) and 16.3 min (GO-1) at 1.0 N. This suggests that GO coatings formed by different dispersion methods have different friction properties, even though they all come from the same source. The friction life of GO-4 is significantly higher than that of GO-1.

The wear traces of GO-based coatings are investigated during both the frictional stabilization period (10 min) and the wear through. Fig. 5a-d show the AFM images, SEM morphology and corresponding Raman mapping of the wear traces of GO-1, GO-2, GO-3 and GO-4 during the friction stabilization period (0.5 N). It is clear that the lubricant film width increases gradually from GO-1 to GO-4. With different colors in the Raman mapping representing different I_D/I_G values. The GO in unworn areas is light blue and has an $I_D/I_G \approx 1.0$. The high I_D/I_G indicates that some of the GO carbon atoms on the six-membered rings form sp^3 hybrid bonds with oxygen, increasing the degree of disorder [45]. Therefore, the GO in the wear trace has an overall bright green color with an $I_D/I_G \approx 1.1$, indicating that mechanical friction increases the defects in the GO flakes. The thickness of the lubrication films is further determined as 160 nm (GO-1), 264 nm (GO-2), 272 nm (GO-3) and 441 nm (GO-4). In addition, the lubrication films are not perfectly flat. It is found that the lubrication films of GO-1, GO-2 and GO-3 contains irregular cracks, but the lubrication film of GO-4 is overall smooth. Similar results are obtained in the wear-through experiments, as shown in Fig. 5e-h, where a small number of flakes appears in the wear traces of GO-1 and GO-2, but intermittent lubricant films remained in GO-3 and GO-4 (Fig.S9). We roughly measure the thickness of the lubrication film as 22 nm (Ra = 27 nm), 74 nm (Ra = 29 nm), 91 nm (Ra = 30 nm) and 161 nm (Ra = 52 nm) for GO-1, GO-2, GO-3 and GO-4. Therefore, different ultrasonic frequency treatments affect the size of the flakes and hence their tribological properties of their coatings; smaller GO are more resistant to wear and their lubricant film is larger, thicker and denser.

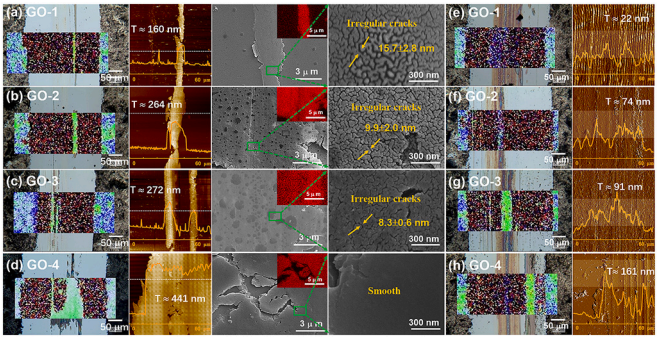

Fig. 5. The wear track of GO-1, GO-2, GO-3 and GO-4 coatings under frictional stabilization period (10 min, a-d) and after wear through (e-h) at 0.5 N load. (Raman mapping of I_D/I_G; SEM and AFM images).

3.3. Microscopic wear resistance of GO-based coatings

Based on the above study, the effect of ultrasonic frequency on the size of GO flakes is the most significant, therefore GO with carbon content of 300 (GO-300) and 100 (GO-100) are selected for the MD simulations to investigate the effect of flake size on its tribological properties. The MD simulation process is divided into three stages, surface enrichment, load down and sliding [46].

The enrichment process of the GO-300 and GO-100 on the Fe surface, the beginning of enrichment and the equilibrium are shown in Fig. 6(a). It is obvious that flakes are enriched towards the substrate, indicating that GO has a better affinity with Fe. Compared with GO-100, GO-300 is more agglomerated, and the distribution of the flakes on the upper and lower surfaces is extremely heterogeneous, with only one lamella on the upper layer and five on the lower layer. The bonding of the flakes to the substrate is positively correlated with the distance them. As shown in the density distribution of the flakes along the *Z*-axis after enrichment equilibrium, and it is found that the lamellae size does not have much effect on its their bonding to the Fe surface, which is manifested by a small difference in the distance between the flakes and the metal surface, about 3.75 Å and 3.72 Å. Although the bonding of the GO-300 and GO-100 to substrate is similar, there is a large different in the degree of coverage of the substrate surface. The topography of the flakes at the top and bottom of the substrate is shown in Fig. 6b. We have labeled each flake in the GO-300 and GO-100 (Fig. S9). For GO-300, layers 1, 4, 5, and 6 are fully spread on the substrate, while layers 2 and 3 form an overlapping structure with a small substrate contact area, thus leaving many uncovered areas on the substrate. For GO-100, the layers 1, 2, 3, 4, 5, 6, 7, 8, 11, 12, 13, 14, 15 and 16 are all fully spread on the Fe surface, with very little uncovered areas on the Fe surface. Thus, smaller nanolayers may have a larger overall contact area with the Fe substrate surface and exhibit better substrate bonding. Similar results are obtained for the statistics of the total energy and van der Waals force changes. As shown in Fig. 6 (c), the total energy and van der Waals force of GO-100 are lower than those of GO-300, implying that GO-100 system is more stable, which may be related to the better coverage of GO-100.

Under loading (0.2 GPa), the distribution density of flakes increases significantly. As shown in Fig. 6 (d), most of the flakes in the coating are flat on the substrate, but there are still some that are vertically aligned, which are burrs on the coating surface, such as layer 6 in GO-300. Further statistics on the change in flake layer spacing before and after pressures show that moderate loading does not lead to a decrease in layer spacing. Instead, the layer spacing of GO-100 (6.41 Å) is smaller than that of GO-300 (7.13 Å), which is mainly attributed to the fact that the larger flakes are more prone to forming an irregular structure with higher spatial potential resistance, resulting in a relatively larger layer spacing. At the same time, the densities of the coatings formed by larger sized flakes decreases due to spatial site resistance (Fig. 6(f)). The densities of the GO-100 and GO-300 are 4.117 and 3.984, which suggests that smaller GO form a denser coating. Further investigating the mean square displacement (MSD) of the flakes in the pressurized systems, the diffusion coefficients of GO-100 (1.11×10^{-12} m^2/s) are much larger than those of GO-300 (4.91×10^{-13} m^2/s), suggesting that smaller GO are more likely to self-repair the defective area during subsequent friction, which is macroscopically reflected in better lubrication film

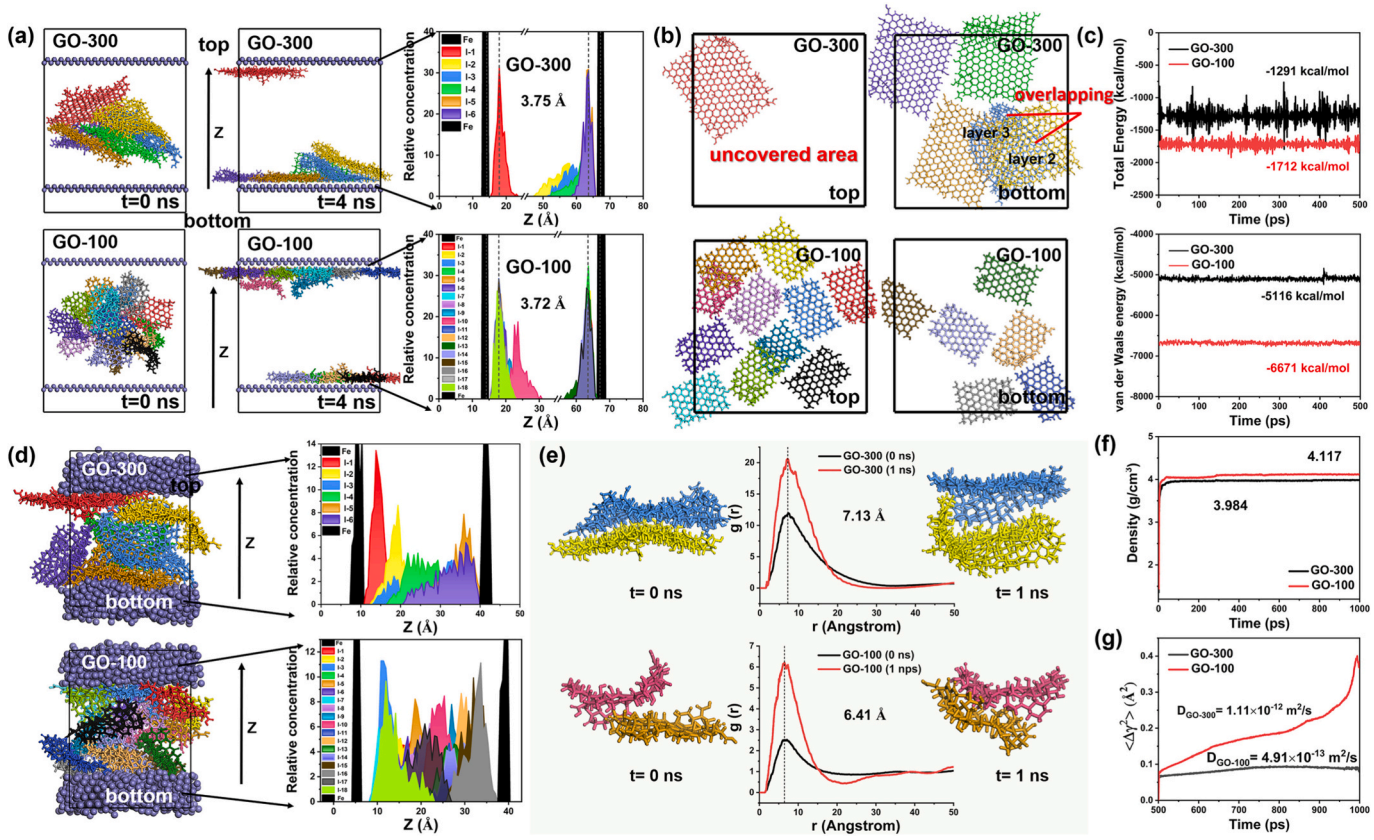

Fig. 6. (a-b) Frontal and lateral morphology and nanolayer distributions of GO-100 and GO-300 at the beginning of enrichment and after equilibrium. (c) Total energy and van der Waals force of the GO-100 and GO-300 during enrichment. (d-f) Snapshots, nanolayer distributions, flakes spacing and density of GO-100 and GO-300 under 0.2 GPa. (e) Mean square displacement of C atoms in the GO-100 and GO-300 (500 ps to 1000 ps).

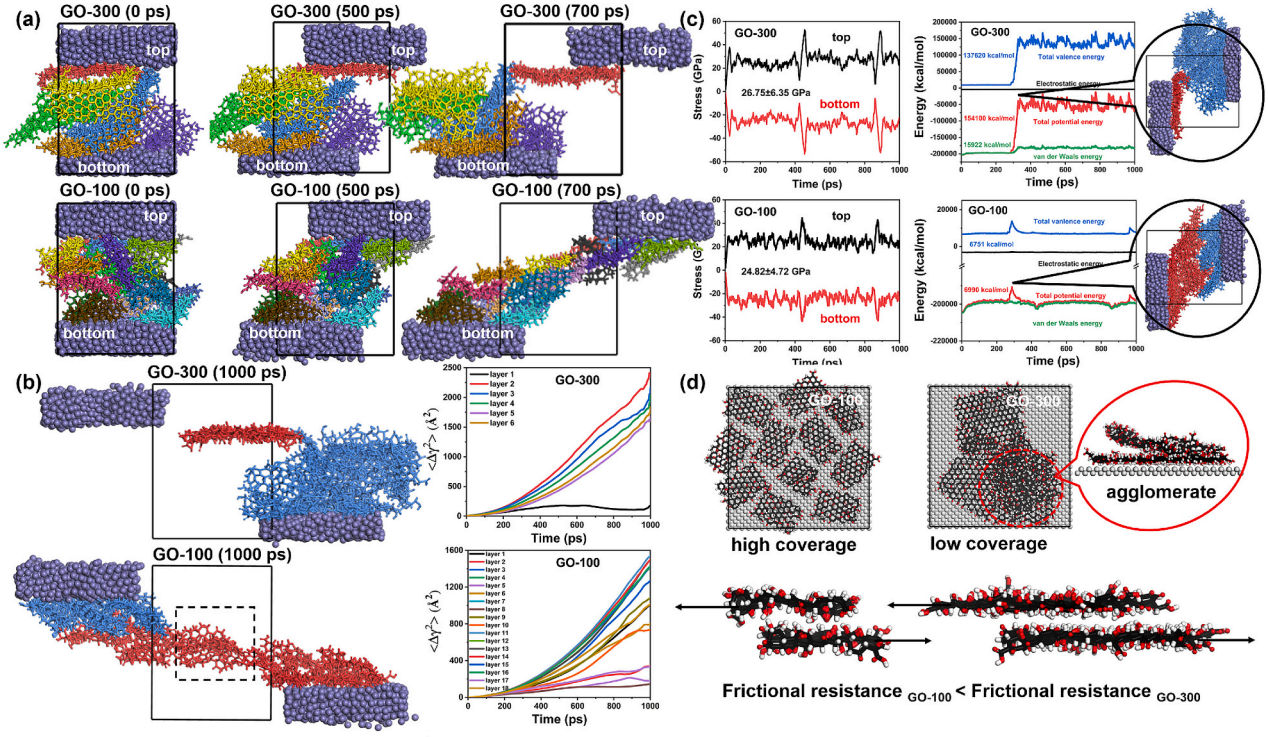

Fig. 7. (a-b) Morphology of the GO-300 and GO-100 during slip (0 ps, 500 ps and 700 ps) and after misalignment (1000 ps) and the MSD of its corresponding flakes. (c) Electrostatic energy, total potential energy, total valence energy and van der Waals energy of the GO-100 and GO-300. (d) Schematic of the mechanism for better wear resistance of GO-100.

continuity.

The above equilibrium pressurized GO-100 and GO-300 are subjected to confined shear with a Fe surface velocity of 4×10^{-4} m/s. The structure evolution of the coating at 0 ps, 500 ps and 700 ps are shown in Fig. 7a [47]. With the relative movement of the Fe substrate, the flakes in both the GO-300 and GO-100 moved obviously, but in a much different way. For GO-300, a significant misalignment occurs during friction, where layer 1 is one slip surface, and layer 2–6 are the other slip surface. It is worth noting that in the previous study layer1 is adsorbed on the top Fe, while layer 2–6 are adsorbed on the bottom Fe, meaning that the flakes adsorbed on the top and bottom do not form a whole during the compression process, and there is still a large gap between them. The MSD curves of layer 1 and layer 2–6 are also difference. And the clusters composed of layer 2–6 do not have much structural variation throughout the friction. On the contrary, GO-100 does not have an obvious slip surface. The morphology of GO-100 at fracture is shown in Fig. 7(b), where the flake initially absorbed on the bottom remains on the top after friction, suggesting that the GO-100 have a better bonding between themselves without aggregation. The MSD curves for the corresponding GO-100 are also very similar. Further statistics on the stress (y-axis direction) and energy changes (electrostatic energy, total potential energy, total valence energy and van der Waals energy) of the system during friction are shown in Fig. 7(c). The average stress of GO-300 and GO-100 in the y-axis during friction are 265.75 ± 6.35 GPa and 24.82 ± 4.72 GPa and it is obvious that the frictional resistance between GO-300 is greater than that of GO-100. Similar results are obtained for the total potential energy and total valence energy of the system, with the total potential energy of GO-300 rising by 136,720 kcal/mol during slip due to flake misalignment (340 ps), whereas that of the GO-100 only rises by 6990 kcal/mol (288 ps), suggesting that the friction between larger GO is greater. In addition, the larger contribution to the above increase in total potential energy is the total valence energy, and the rise in van der Waals forces is not significant, especially for GO-100, which is essentially unchanged. Thus, we believe that the friction between GO flakes mainly originates from the hindering force caused by covalent bond deformation due to lamellar misalignment, and the hindering force can gradually disappear through the change of flake displacement, so the smaller flakes not only have small hindering force for covalent bond deformation, but also can be disappeared by the rapid movement, which is reflected in the overall smaller friction.

According to the above study, the main reasons for better wear resistance of smaller flakes are as follows (as shown in Fig. 7(d)): 1. smaller flakes have a larger coverage area on the Fe surface and thus show stronger substrate bonding; 2. smaller flakes form a more homogeneous coating without larger aggregates, which is less likely to be faulted during friction; 3. smaller flakes have less covalent bond deformation and van der Waals forces during friction, resulting in less overall sliding resistance.

4. Conclusion

In this paper, GO-1 (mechanical stirring, 2 h), GO-2 (10 kHz, 2 h), GO-3 (20 kHz, 2 h) and GO-4 (40 kHz, 2 h) are prepared according to different dispersion methods and ultrasonic frequencies. It is found that the dispersion method has little effect on the chemical properties of GO (except for a slight increase in the content of epoxy groups on the surface of the flake with increasing ultrasound frequency), but a very strong effect on the number of layers and the size of the flake. Where the number of flake layers of GO-1, GO-2, GO-3 and GO-4 are 4–6, 2–4, 1–2 and 1, and their areas are 1691.7 ± 1148.6 μm^2, 313.0 ± 144.7 μm^2, 48.0 ± 17.5 μm^2 and 20.7 ± 7.8 μm^2. For the friction test, the friction life of GO-1, GO-2, GO-3 and GO-4 coatings at 0.5 N are17.1 min, 21.7 min, 32.5 min and 48.6 min, and the corresponding lubrication films thickness are 160 nm, 264 nm, 272 nm and 441 nm, which indicates that smaller GO are more wear-resistant and have larger, thicker and denser lubrication films. MD simulations are further used to investigate the microscopic mechanism for better wear resistance of smaller GO. It is found that in the enrichment stage, the smaller GO has better coverage on the Fe surface, and the overall bonding of the corresponding coating is stronger. In addition, the van der Waals forces of smaller flakes are not strong enough to form large particle agglomerates, resulting in a denser and more uniform coating. During friction, smaller flakes have less covalent bond deformation and van der Waals forces, resulting in less sliding resistance. And the smaller flakes are easier to move in the friction process, which can achieve the self-repair of the damaged parts. However, in terms of friction and wear properties, higher ultrasonic frequency and longer ultrasonic time during the dispersion of nanomaterials may be more favourable to improve the wear resistance of their corresponding coatings.

CRediT authorship contribution statement

Chang Tu: Writing – review & editing, Validation, Resources. **Rui Yuan:** Project administration, Funding acquisition, Data curation. **Huiping Qi:** Validation, Formal analysis, Conceptualization. **Lei Chen:** Resources, Investigation, Data curation. **Xiaoyuan Qin:** Supervision, Software, Conceptualization. **Jing Yuan:** Formal analysis, Data curation.

Declaration of competing interest

The authors declare that they have no known competing financial interests or personal relationships that could have appeared to influence the work reported in this paper.

Acknowledgement

This work is financially supported by the National Natural Science Foundation of China No. 52265027; Natural Science Foundation of Qinghai Province (No. 2024-ZJ-794).

Appendix A. Supplementary data

Supplementary data to this article can be found online at https://doi.org/10.1016/j.surfcoat.2025.131737.

Data availability

Data will be made available on request.

References

[1] P. Li, W. He, P. Ju, L. Ji, X. Liu, F. Wu, Z. Lu, H. Li, L. Chen, J. Liu, H. Zhou, J. Chen, Acquisition of molecular rolling lubrication by self-curling of graphite flake at cryogenic temperature, Nat. Commun. 15 (1) (2024) 1–9.
[2] S. Fan, Y. Chen, J. Wu, S. Xiao, G. Chen, P.K. Chu, Structure, superlubricity, applications, and chemical vapor deposition methods of graphene solid lubricants, Tribol. Int. 198 (2024) 109896.
[3] F. Zhou, J. Shan, L. Cui, Y. Qi, J. Hu, Y. Zhang, Z. Liu, Direct plasma-enhanced-chemical-vapor-deposition syntheses of vertically oriented graphene films on functional insulating substrates for wide-range applications, Adv. Funct. Mater. 32 (42) (2022) 2270236.
[4] D. Berman, L.I. Farfan-Cabrera, A. Rosenkranz, A. Erdemir, Advancing the frontiers of EV tribology with 2D materials–a critical perspective, Mater. Sci. Eng. R. Rep. 161 (2024) 100855.
[5] D. Berman, L.I. Farfan-Cabrera, A. Rosenkranz, A. Erdemir, 2D materials for durable and sustainable electric vehicles, Nature Reviews Materials (2024) 1–3.
[6] M. Marian, C.D.Q. Esteban, D.F. Zambrano, S.M. Ramteke, J.R. Grez, B.C. Wyatt, J. Patenaude, B.G. Wright, B. Anasori, A. Rosenkranz, Ti3C2Tx and Mo2TiC2Tx MXenes as additives in synovial fluids-towards an enhanced biotribological performance of 3D-printed implants, Appl. Mater. Today 41 (2024) 102464.
[7] D. Berman, A. Erdemir, A.V. Zinovev, A.V. Sumant, Nanoscale friction properties of graphene and graphene oxide, Diam. Relat. Mater. 54 (2015) 91–96.
[8] B. Jin, J. Zhao, Y. He, G. Chen, Y. Li, C. Zhang, J. Luo, High-quality ultra-flat reduced graphene oxide flakes with super-robust lubrication performances, Chem. Eng. J. 438 (2022) 135620.
[9] O. Hod, E. Meyer, Q. Zheng, M. Urbakh, Structural superlubricity and ultralow friction across the length scales, Nature 563 (7732) (2018) 485–492.

[10] X. Gao, J. Zhang, P. Ju, J. Liu, L. Ji, X. Liu, T. Ma, L. Chen, H. Li, H. Zhou, J. Chen, Shear-induced interfacial structural conversion of graphene oxide to graphene at macroscale, Adv. Funct. Mater. 30 (46) (2020) 2004498.
[11] X. Yang, R. Li, Y. Wang, J. Zhang, Tunable, wide-temperature, and macroscale superlubricity enabled by nanoscale Van Der Waals heterojunction-to-homojunction transformation, Adv. Mater. 35 (39) (2023) 2303580.
[12] R. Li, C. Sun, X. Yang, Y. Wang, K. Gao, J. Zhang, J. Li, Toward high load-bearing, ambient robust and macroscale structural superlubricity through contact stress dispersion, Chem. Eng. J. 431 (2022) 133548.
[13] R. Li, X. Yang, J. Zhao, C. Yue, Y. Wang, J. Li, E. Meyer, J. Zhang, Y. Shi, Operando formation of Van der Waals heterostructures for achieving macroscale superlubricity on engineering rough and worn surfaces, Adv. Funct. Mater. 32 (18) (2022) 2111365.
[14] Y. Liu, X. Chen, J. Li, J. Luo, Enhancement of friction performance enabled by a synergetic effect between graphene oxide and molybdenum disulfide, Carbon 154 (2019) 266–276.
[15] R. Li, X. Yang, M. Ma, J. Zhang, Hydrogen-enhanced catalytic conversion of amorphous carbon to graphene for achieving superlubricity, Small 19 (10) (2023) 2206580.
[16] S. Fan, S. Xiao, S. Lin, F. Su, Y. Su, P.K. Chu, Macroscale superlubricity and durability of in situ grown hydrogenated graphene coatings, Chem. Eng. J. 459 (2023) 141521.
[17] C. Keller, G. Barbillon, C. Debiemme-Chouvy, O. Sel, H. Perrot, Hydrothermal vs. Electrochemical reduction of graphene oxide: a physico-chemical and quartz crystal microbalance study, Carbon 227 (2024) 119246.
[18] W. Cheng, W. Zhang, J. Tao, F. Zheng, B. Chu, R. Wang, C. Fang, L. Huai, P. Tao, C. Song, W. Shang, B. Fu, T. Deng, Octopus-like microstructure of graphene oxide generated through laser–microdroplet interaction for adhesive coating, ACS Nano 18 (11) (2024) 7877–7889.
[19] M. Daly, C. Cao, H. Sun, Y. Sun, T. Filleter, C.V. Singh, Interfacial shear strength of multilayer graphene oxide films, ACS Nano 10 (2) (2016) 1939–1947.
[20] X. Gao, L. Chen, L. Ji, X. Liu, H. Li, H. Zhou, J. Chen, Humidity-sensitive macroscopic lubrication behavior of an as-sprayed graphene oxide coating, Carbon 140 (2018) 124–130.
[21] A.Z. Macknojia, A. Ayyagari, E. Shevchenko, D. Berman, MXene/graphene oxide nanocomposites for friction and wear reduction of rough steel surfaces, Sci. Rep. 13 (1) (2023) 11057.
[22] Z. Chen, M. Zhang, P. Ren, Z. Lan, Z. Guo, H. Yan, Y. Jin, F. Ren, Enhanced mechanical and tribological properties of epoxy composites reinforced by novel hyperbranched polysiloxane functionalized graphene/MXene hybrid, Chem. Eng. J. 466 (2023) 143086.
[23] W. Wang, Y. Zhang, Z. Li, L. Qian, Controllable friction on graphene via adjustable interfacial contact quality, Advanced Science 10 (30) (2023) 2303013.
[24] T. Wang, X.-X. Tian, Y.-W. Li, J. Wang, M. Beller, H. Jiao, Coverage-dependent CO adsorption and dissociation mechanisms on iron surfaces from DFT computations, ACS Catal. 4 (6) (2014) 1991–2005.
[25] A. Boda, S.M. Ali, K.T. Shenoy, S. Mohan, Adsorption, absorption, diffusion, and permeation of hydrogen and its isotopes in bcc bulk Fe and Fe(100) surface: plane wave-based density functional theoretical investigations, J. Phys. Chem. C 123 (39) (2019) 23951–23966.
[26] R. Yuan, L. Gao, J. Liu, C. Tu, R. Tan, S. Xu, Effect of hydrophobic alkyl chains on the plasticization properties of citrate: experiments and MD simulation, Eur. Polym. J. 203 (2024) 112644.
[27] Y. Shi, J. Pu, L. Wang, Structural phase transformation in amorphous molybdenum disulfide during friction, J. Phys. Chem. C 125 (1) (2020) 836–844.
[28] G. Tang, Z. Wu, F. Su, H. Wang, X. Xu, Q. Li, G. Ma, P.K. Chu, Macroscale superlubricity on engineering steel in the presence of black phosphorus, Nano Lett. 21 (12) (2021) 5308–5315.
[29] S. Liao, Q. Ke, Y. Wei, L. Li, Water-Graphene non-bonded interaction parameters: development and influence on molecular dynamics simulations, Appl. Surf. Sci. 603 (2022) 154477.
[30] M. Reil, J. Hoffman, P. Predecki, M. Kumosa, Intermolecular interactions in graphene and oxidized graphene nanocomposites, Compos. Sci. Technol. 248 (2024) 110433.
[31] W. Hao, C. Sui, G. Cheng, J. Li, L. Miao, G. Zhao, Y. Sang, J. Li, C. Zhao, Y. Zhou, Z. Zang, Y. Zhao, X. He, C. Wang, Dynamic insights into the growth mechanisms of 2D covalent organic frameworks on graphene surfaces, ACS Nano 18 (15) (2024) 10485–10494.
[32] R. Yuan, L. Ji, Y. Wu, H. Li, P. Ju, L. Chen, H. Zhou, J. Chen, "Plate-anchor" shaped POSS-functionalized graphene oxide with self-fixing effect in polyimide matrix: molecular dynamic simulations and experimental analysis, Compos. Sci. Technol. 176 (2019) 103–110.
[33] Y. Yang, F. Zheng, L. Wang, Y. Liu, 3D MoS2/graphene oxide integrated composite as anode for high-performance sodium-ion batteries, Sci. Rep. 14 (1) (2024) 19231.
[34] R. Yuan, P. Li, L. Chen, J. Yuan, B. Xu, G. Sun, E. Ding, J. Chen, Effects of grafting oxygen atoms on the tribological properties of graphene: molecular dynamics simulation and experimental analysis, Appl. Surf. Sci. 528 (2020) 147045.
[35] C. Tang, Y. Jiang, L. Chen, J. Sun, Y. Liu, P. Shi, J.Y. Aguilar-Hurtado, A. Rosenkranz, L. Qian, Layer-dependent nanowear of graphene oxide, ACS Nano 17 (3) (2023) 2497–2505.
[36] W.H. Lee, S.A.F. Bon, Branched polymer grafted graphene oxide (GO) as a 2D template for calcium phosphate growth, J. Colloid Interface Sci. 675 (2024) 438–450.
[37] W. Li, C. Li, H. Yang, H. Yang, J. Qu, Y. Han, X. Li, Z.-Z. Yu, Well-designed lamellar reduced graphene oxide-based foam for high-performance solar-driven water purification, J. Colloid Interface Sci. 660 (2024) 716–725.
[38] R. Shu, L. Xu, Y. Guan, Preparation of cellulose derived carbon/reduced graphene oxide composite aerogels for broadband and efficient microwave dissipation, J. Colloid Interface Sci. 675 (2024) 401–410.
[39] Y. Seon Lee, N. Ryeol Kim, S. Ki Park, Y.-i. Ko, Y. Shin, B. Yang, C.-M. Yang, Effects of high-temperature thermal reduction on thermal conductivity of reduced graphene oxide polymer composites, Appl. Surf. Sci. 650 (2024) 159140.
[40] S. Yin, H. Wu, X. Yi, Z. Huang, C. Ye, P. Li, Y. Zhang, J. Shi, K. Hua, H. Wang, Enhanced graphene oxide adhesion on steel surface through boronizing functionalization treatment: Toward the robust ultralow friction, Carbon 206 (2023) 201–210.
[41] K. Ge, H. Shao, E. Raymundo-Piñero, P.-L. Taberna, P. Simon, Cation desolvation-induced capacitance enhancement in reduced graphene oxide (rGO), Nat. Commun. 15 (1) (2024) 1935.
[42] E.M. Mostafa, A. Ghanem, R. Hosny, R. El-Nagar, In-situ upgrading of Egyptian heavy crude oil using matrix polymer carboxyl methyl cellulose/silicate graphene oxide nanocomposites, Sci. Rep. 14 (1) (2024) 20985.
[43] X. Ge, L. Zhang, Q. Shi, Y. Xing, Y. Liu, Z. Cao, W. Wang, Facilitating macroscopic superlubricity through electric stimulation with graphene oxide flake additives for steel surface lubrication, Appl. Surf. Sci. 661 (2024) 160039.
[44] P. Gong, J. Li, J. Wang, W. Wu, C. Li, D. Wang, J. Shi, J. Liu, F. Zhou, W. Liu, Controlled growing of graphdiyne film for friction reduction and antiwear, ACS Nano 17 (9) (2023) 8252–8261.
[45] C. Chen, P. Xue, D. Diao, Graphitization vs tribo-oxidation governing friction behaviors of doped graphene nanocrystalline carbon films, Carbon 197 (2022) 435–443.
[46] L. Frérot, A. Crespo, J.A. El-Awady, M.O. Robbins, J. Cayer-Barrioz, D. Mazuyer, From molecular to multiasperity contacts: how roughness bridges the friction scale gap, ACS Nano 17 (3) (2023) 2205–2211.
[47] N. Baig, I. Abdulazeez, N.A. Khan, M.B. Hanif, Experimental and theoretical assessment of bioinspired next-generation intercalated graphene oxide-based ceramic membranes for oil-in-water emulsion separation, npj Clean Water 7 (1) (2024) 82.